Available online at www.sciencedirect.com
SCIENCE DIRECT®
Coordination Chemistry Reviews 248 (2004) 1381–1389
COORDINATION CHEMISTRY REVIEWS
www.elsevier.com/locate/ccr

Review

Significant influence of TiO_2 photoelectrode morphology on the energy conversion efficiency of N719 dye-sensitized solar cell

Zhong-Sheng Wang [a], Hiroshi Kawauchi [b], Takeo Kashima [b], Hironori Arakawa [c,*]

[a] *Photoreaction Control Research Center (PCRC), National Institute of Advanced Industrial Science and Technology (AIST), 1-1-1, Higashi, Tsukuba, Ibaraki 305-8565, Japan*
[b] *Material Research Laboratory, Furukawa Co. Ltd., 1-25-3, Kannondai, Tsukuba, Ibaraki 305-0856, Japan*
[c] *Department of Industrial Chemistry, Faculty of Engineering, Tokyo University of Science (Tokyo Rika Daigaku) 1-3, Kagurazaka, Shinjyuku-ku, Tokyo, 162-8601, Japan*

Received 22 December 2003; accepted 18 March 2004
Avaibable online 12 May 2004

Contents

Abstract 1381
1. Introduction 1381
2. Experimental section 1382
   2.1. Preparation of TiO_2 particles 1382
   2.2. Fabrication of photoelectrodes with different morphologies 1383
   2.3. Photovoltaic measurements 1384
3. Results and discussion 1384
   3.1. Monolayer 1384
   3.2. Double layer 1386
   3.3. Multilayer 1387
4. Conclusions 1388
Acknowledgements 1388
References 1388

Abstract

Since Grätzel's group reported an overall efficiency of 10% for dye-sensitized solar cell using *cis*-di(thiocyanato)bis(2,2′-bipyridyl-4,4′-dicarboxylate)ruthenium(II), many other institutions have tried to reproduce it. However, no other institutions have, so far, reported such a high efficiency. In order to develop high efficiency dye-sensitized solar cells, the tuning of TiO_2 photoelectrode morphology towards optimization of solar energy conversion efficiency has been investigated. TiO_2 photoelectrodes with six different structures, with layers of nanoparticles, light-scattering particles, and mixture of nanoparticles and light-scattering particles on the conducting glass at a desirable sequence and thickness, were designed and investigated. The profiles of photocurrent action spectra were compared in terms of light scattering and the suppression of light loss due to the back-scattering of large particles near the conducting glass. The data show that the multilayer structure is superior to the mono- and double-layer structure, with ∼85% of incident monochromatic photon-to-electron conversion efficiency (IPCE) below 620 nm and ∼45% of IPCE at 700 nm. The solar-to-electric energy conversion efficiency of N719 dye-sensitized solar cell has been improved significantly from 7.6 to 9.8% by tuning the film structure from monolayer to multilayer. The best efficiency of 10.2% under illumination of simulated AM1.5 solar light (100 mW cm^{-2}) was attained with a multilayer structure using an anti-reflection film on the cell surface.

Keywords: Dye-sensitized solar cells; TiO_2 photoelectrode; Morphology; Light scattering; N719 ruthenium complex

1. Introduction

Dye-sensitized solar cells (DSSCs) [1], which emerged as a new generation photovoltaic device, have been studied extensively [2–6] because of their high efficiency and low-cost. The two outstanding sensitizers for DSSC so

* Corresponding author. Tel.: +81-3-5228-8311; fax: +81-3-5261-4631.
E-mail address: h.arakawa@ci.kagu.tus.ac.jp (H. Arakawa).

0010-8545/$ – see front matter © 2004 Elsevier B.V. All rights reserved.
doi:10.1016/j.ccr.2004.03.006

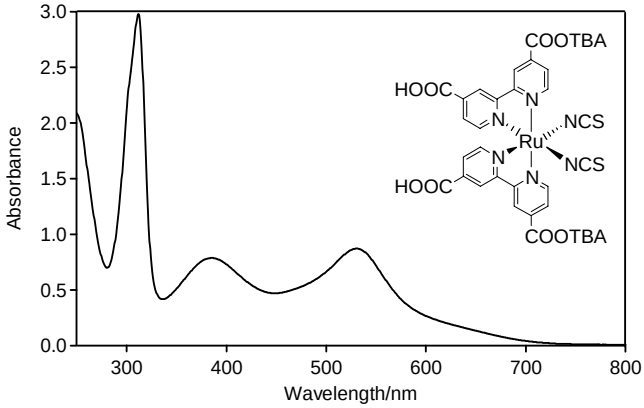

Fig. 1. UV–Vis absorption spectrum of N719 in 1:1 acetonitrile and *tert*-butanol. The inset shows the molecular structure of N719.

far reported are *cis*-di(thiocyanato)bis(2,2′-bipyridyl-4,4′-dicarboxylate)rut-henium(II) [7], so called N719 (Fig. 1), and tri(thiocyanato)-2,2′,2″-terpyridyl-4,4′,4″-tricarboxylate)ruthenium(II) [8], so called the black dye. The highest efficiencies reported for N719 and the black dye are 10 and 10.4%, respectively [7,8], which is comparable to the conventional silicon-based solar cell. In particular, N719 has emerged as the standard dye to compare and select other new sensitizers for DSSC [9–11], because it has not only a high efficiency but also a high photo- and chemical-stability.

The maximum energy conversion efficiency (η_{global}) of N719 in AM1.5 sun can be estimated from the integral photocurrent density (J_{sc}), the open-circuit photovoltage (V_{oc}), the fill factor (FF), and the power of the incident light (P, 100 mW cm^{-2}).

$$\eta_{global} = \frac{J_{sc} V_{oc} FF}{P} \quad (1)$$

J_{sc} can be calculated by the overlap integration of global AM1.5 solar emission spectrum and the photocurrent action spectrum over the wavelengths where the dye absorbs.

$$J_{sc} = \int qF(\lambda)[1 - r(\lambda)]IPCE(\lambda)d\lambda \quad (2)$$

where q is the electron charge, $F(\lambda)$ the incident photon flux density at wavelength λ, $r(\lambda)$ the incident light loss due to the light absorption and reflection by conducting glass, and IPCE(λ) is defined as the incident monochromatic photon-to-electron conversion efficiency. IPCE(λ) can be obtained through the following expression:

$$IPCE(\lambda) = \frac{1240 \times J_{sc}\ (\mu A\ cm^{-2})}{\lambda\ (nm) \times P\ (W\ m^{-2})} \quad (3)$$

J_{sc} can be deduced to be ~20 mA cm^{-2} using 0.1 of $r(\lambda)$ and an average IPCE value of 0.85. As a consequence, the theoretical energy conversion efficiency of N719 is estimated to be around 14% using a V_{oc} of 0.9 V and FF of 0.8 [12]. In addition, the 10% efficiency for N719 has not been reproduced by institutions other than Grätzel's group, and the usually reported values are only around 8.4% [13,14]. For these reasons, there have been more and more efforts on the improvement of N719-based DSSCs through the optimizations of dye, TiO_2 surface, and electrolytes [14–16]. Although the high surface area of a nanocrystalline film meets the requirement of adsorbing large amount of dyes in the monolayer, it brings about, at the same time, many opportunities for the recombination of photoinjected electrons and the oxidized dye and/or the electron acceptors in the electrolyte. However, the small size of the individual nanoparticles cannot support a space charge layer, which is essential for charge separation in bulk semiconductor [17]. It has recently been reported that an insulated layer coating on the surface of mesoporous film could retard the interfacial recombination process and remarkably improve the DSSC performance due to the formation of an energy barrier at the electrode and electrolyte interface [18–20]. These improvements turned out to be remarkable, but the final efficiencies announced were well below 6% [18,19], still much lower than the already reported efficiency of 10% [7]. From this point of view, the surface coating by insulating layers is still unsuccessful. In order to develop high efficiency DSSCs, optimizing information for the photoelectrode is highly desirable, because Grätzel and co-workers [7] did not describe the TiO_2 film morphology in detail for obtaining 10% efficiency.

There are many factors limiting the cell performance, among which light harvesting efficiency is very important. Since N719 has low absorption in the red region (Fig. 1), large particles, with light-scattering effect, are incorporated into the film to enhance the photoresponse to red light. However, the reduction of surface area and light loss due to back-scattering arising from the presence of large particles counteract the light-scattering effect [21–23]. This article discusses methods to balance the light scattering and surface area effects, which are opposed to each other. To harvest visible light efficiently, a multilayer structure was proposed in our group. Herein, we outline the tuning of layer structures and their effect on the performance of DSSC.

2. Experimental section

2.1. Preparation of TiO_2 particles

The DSSC performance depends on the nature and size of the TiO_2 particles. TiO_2 particles must be prepared with good dispersion and high crystallinity. Since anatase is better than rutile and brookite for solar energy conversion, the anatase phase is favorable in the preparation of TiO_2 particles, and the other two phases, rutile and brookite, should be avoided.

Three kinds of TiO_2 particles were prepared in a basic environment according to the procedure reported [24], which was modified as follows. Titanium tetraisopropoxide (TTIP) was added to water (Ti:H_2O = 1:50) at 15 °C under vigorous stirring for 1 h. The white precipitate so formed was filtered and washed three times with water. It was then transferred to a tetramethylammonium hydroxide (TMAH) solu-

Table 1
BET surface area and average particle size of the prepared TiO_2 particles

TiO_2 particles	Surface area ($m^2\,g^{-1}$)	d_{BET} (nm)[a]
N[b]	66.3	23.3
S1[c]	30.4	50.7
S2[d]	15.4	100.2

[a] Average diameter of TiO_2 particles were calculated from the BET surface area, assuming the particles are spherical.
[b] N stands for nanoparticles. The molar ratio of TTIP to TMAH was set at 62.5:1.
[c] S1 stands for the 50 nm particles. The molar ratio of TTIP to TMAH was set at 250:1.
[d] S2 stands for the 100 nm particles. The molar ratio of TTIP to TMAH was set at 500:1.

tion and refluxed at 100 °C for 4 h under stirring. The content of TiO_2 was set at 10 wt.%. The resultant colloids were heated at 270 °C for 4 h in a titanium autoclave under stirring. TiO_2 particles with different sizes were obtained when the molar ratio of TMAH to Ti was varied. The TMAH content has a large influence on the Brunauer–Emmett–Teller (BET) surface area and the particle size; the results are summarized in Table 1. The surface area decreased and particle size increased with decreasing content of TMAH in the range tested, and vice versa. The average diameters of the TiO_2 particles obtained were 23, 50, and 100 nm (see Table 1).

Fig. 2 shows the XRD patterns of nanoparticles (23 nm), large particles (50 nm), and the larger particles (100 nm).

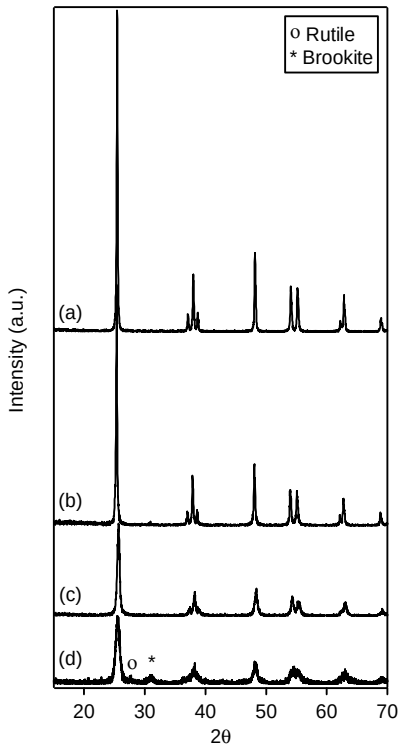

Fig. 2. XRD patterns of TiO_2 powders. (a) Large particles (100 nm) obtained at Ti:TMAH = 500, where TMAH, tetramethylammonium hydroxide, (b) large particles (50 nm) obtained at Ti:TMAH = 250, (c) nanoparticles (23 nm) obtained at Ti:TMAH = 62.5, and (d) nanoparticles (14 nm) obtained from a 0.1 mol dm^{-3} nitric acid solution.

The XRD peaks broaden with increasing TMAH content, indicating a decreased particle size with increasing concentration of TMAH over the range investigated. All the peaks assignable to the anatase phase were clearly observed in the XRD patterns. The XRD peaks were intense and very well resolved, suggesting that the TiO_2 particles obtained have high crystallinity. No peaks for other phases such as rutile and brookite were observed, indicative of pure anatase particles.

The usually employed TiO_2 nanoparticles are synthesized by hydrolysis of TTIP in 0.1 M nitric acid followed by autoclaving at 230 °C [7], and its XRD pattern is also shown in Fig. 2 for comparison. However, TiO_2 nanoparticles prepared in 0.1 M nitric acid contain rutile and brookite impurities [25], which is disadvantageous to solar energy conversion [26]. The surface area for nanoparticles prepared in nitric acid is about 120 $m^2\,g^{-1}$, which is almost double that of the TiO_2 nanoparticles (N) from TMAH. Furthermore, the TiO_2 film fabricated from the former particles can indeed adsorb a larger amount of dye than the film made of the latter particles. The latter photoelectrode could, however, yield a higher efficiency. One possible reason is that TiO_2 particles prepared from TMAH contain pure anatase crystallites and can form as an ordered structure in the film [24]. Frank and co-workers [26] compared the performance of dye-sensitized rutile- and anatase-based TiO_2 solar cells, and concluded that electron transport is slower in the rutile layer than in the anatase layer. As a consequence, the short-circuit photocurrent of the rutile-based cell was lower than that of the anatase-based cell. Their results suggested that rutile or other impurities in TiO_2 photoelectrodes would result in lower performance. In addition, the porosity of the film and the pore dimensions, which are determined in part by the particle size, can influence the transportation kinetics of redox species. If the pores are too small, the diffusion kinetics in the electrolyte will become the limiting step in the photocurrent generation, which, of course, has a significant influence on the overall efficiency [25]. The three kinds of TiO_2 particles prepared from TMAH were employed for fabrication of various photoelectrodes in this article.

2.2. Fabrication of photoelectrodes with different morphologies

TiO_2 films were fabricated using a screen printing method. Nanoparticles, large particles, and mixtures containing nanoparticles and large particles at a ratio of 6:4 were employed to prepare various TiO_2 pastes for screen printing. TiO_2 particles were dispersed in α-terpineol with ethyl cellulose as a binder. The constituents in each TiO_2 paste are listed in Table 2. Paste N and S were composed of nanoparticles (23 nm) and scattering particles (100 nm), respectively. Paste M contained a mixture of nanoparticles and large particles (100 nm) at a ratio of 6:4, and paste M′ was made of a mixture of nanoparticles and particles of 50 nm at a ratio of 6:4 too. Fig. 3 shows the film structure, N, M, NS,

Table 2
Composition (wt.%) of various TiO_2 pastes

Type of pastes	Nanoparticles (23 nm)	S1 (50 nm)	S2 (100 nm)
N	100		
M′	60	40	
M	60		40
S			100

NM, NMS, and NM′MS, studied in this report. Structure N and M, composed of homogeneous nanolayer and mixed layer, respectively, are regarded as a monolayer, whereas structure NS and NM, consisting of two different layers, are regarded as a double layer. Structure NMS and NM′MS contain three or more different layers and are referred to as multilayer. Various layers were printed onto the conducting glass (Nippon Sheet Glass Co., Japan, F-doped SnO_2 layer, 8–10 $\Omega\,\square^{-1}$) sequentially using the paste listed in Table 2. The film thickness was measured with a Tencor Alpha-Step 500 Surface Profiler. The film size was 5 mm × 5 mm, whose geometric area was precisely measured with a Nikon Digital Camera controlled by a computer using an objective micrometer ruler as a reference. Because it is very difficult to grow the film vertically, the projection of the film, measured as the film area, is a little larger than the bottom area of the film. Therefore, the efficiency reported in this article might be underestimated a little.

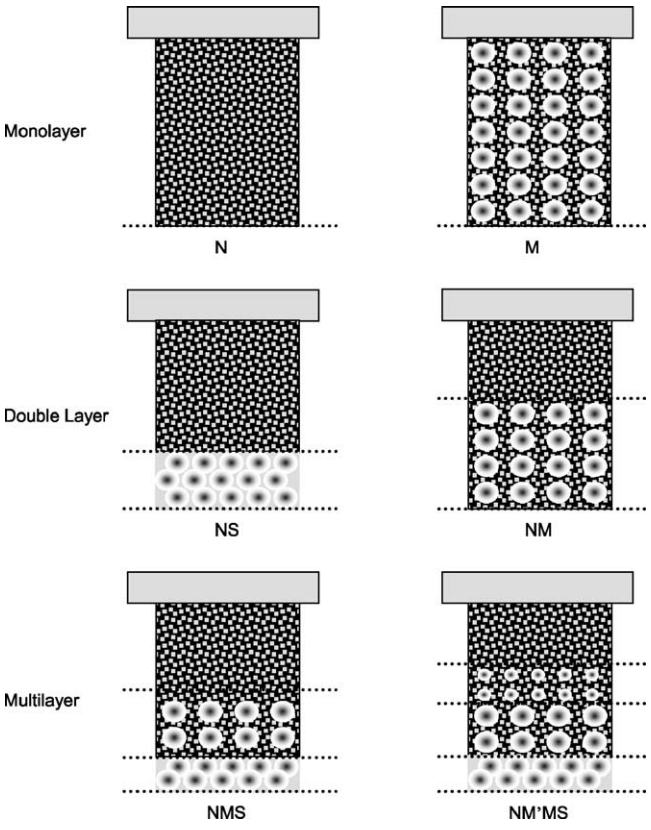

Fig. 3. Schematic film morphologies of studied TiO_2 photoelectrodes.

2.3. Photovoltaic measurements

The TiO_2 photoelectrodes were heated at 525 °C for 2 h under an air atmosphere. After treating the films with 0.05 M $TiCl_4$ for 30 min at 70 °C [8], the films were calcined at 450 °C for 30 min and allowed to cool to 160 °C before immersing them into the dye solution for 4 days. The N719 (Solaronix SA, Switzerland) solution was prepared in a mixed solvent of 1:1 acetonitrile and *tert*-butanol. The concentration was 2×10^{-4} mol dm^{-3}. In order to determine the surface concentration of N719 in the photoelectrode, the dye was desorbed into 0.1 mol dm^{-3} NaOH solution in a mixed solvent (water/ethanol = 1:1, v/v), and the UV–Vis absorption spectrum of the resultant solution, whose molar extinction coefficient was determined to be 1.41×10^4 dm^3 mol^{-1} cm^{-1} at 515 nm, was measured to estimate the adsorbed amount of dye.

The sandwich-type solar cell was assembled by placing a platinum-coated conducting glass (counter electrode) on the N719 dye-sensitized photoelectrode (working electrode), and clipped together as open cells for measurements. On the other hand, sealed cells were also tested in this study. The two electrodes were separated by a surlyn spacer (30 μm thick) and sealed up by heating the polymer frame [13]. The redox electrolyte was introduced into the space of inter-electrodes through the two holes pre-drilled on the back of the counter electrode. The two holes were sealed up using a surlyn film, on which a glass slide was pressed under heat. The redox electrolyte used was 0.1 M LiI, 0.05 M I_2, 0.6 M dimethyl propyl imidazolium iodide, and 0.5 M *tert*-butylpyridine in dried acetonitrile. The current–voltage characteristics of the cells were measured with a source meter (Advantest, R6246). An AM1.5 solar simulator (Yamashita Denso Co., YSS-150A with a 1000-W Xe lamp and an AM1.5 filter) was employed as the light source. The incident light intensity was calibrated with a standard Si solar cell produced by Japan Quality Assurance Organization (JQA). Photocurrent action spectra, IPCE plotted as a function of excitation wavelength, were recorded on a CEP-99W system (Bunkoh-Keiki Co. Ltd.). Four parallel samples for each kind of layer structure were made for *I–V* and IPCE measurement, and the reproducibility of TiO_2 photoelectrode was quite good. It is of note that black painting was applied to the surrounding of the dye-coated film during the measurement; otherwise, the efficiency was 1.3–1.5% higher than the reported one, because more photons from the surrounding part of the film can penetrate to the N719 dye through reflection and refraction of the glass texture.

3. Results and discussion

3.1. Monolayer

At the initial research stage of DSSC, a transparent nanofilm (N) was used to study the cell performance [27]. A

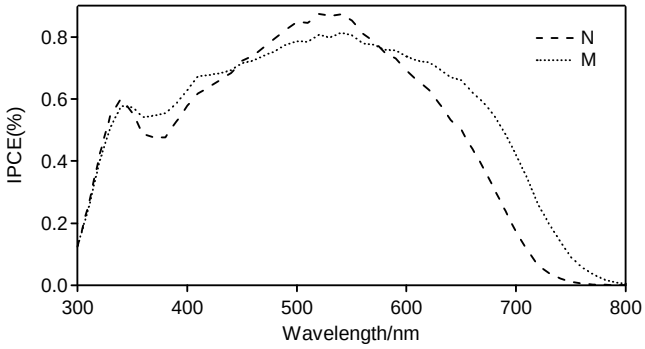

Fig. 4. Photocurrent action spectra of the electrodes with structure N and M.

typical photocurrent action spectrum is illustrated in Fig. 4, which presents a narrow shape with IPCE at 700 nm of 17%. The dramatic decrease in IPCE from 550 nm to longer wavelength is ascribed from the low absorption of N719 in the red region. The nano-film is transparent and has no light scattering. Light loss due to the transmittance of light with wavelength greater than 600 nm accounts for the poor IPCEs in the red region. An open cell of N only generated η of 7.6% due to the low J_{sc} of 14.86 mA cm^{-2} (Table 3). Increasing the film thickness is an easy way to increase the amount of adsorbed dye for the benefit of enhancing the light absorption in the red region, and hence, the IPCEs there. However, the overall efficiency will be decreased in thick films, as discussed below.

In order to improve the absorption above 600 nm, large particles were introduced to the nanoparticles matrix, and structure M shows a broad feature in the action spectrum as a result of the effect of light scattering by the large particles (see Fig. 4). Compared with structure N, structure M extended the photocurrent onset from 750 to 800 nm and remarkably improved the IPCEs above 600 nm. From 800 nm, the IPCE rises gradually until at 620 nm it reaches a plateau of ~80%. The efficient light scattering due to large particles is responsible for the broad feature in the action spectrum of M.

The performance characteristics of sandwiched solar cells of M are also listed in Table 3. Although M adsorbed smaller amount of dyes than N, the former generated a higher J_{sc} due to the much improved IPCEs in the red region. As a result of increased J_{sc}, η increased from 7.6 to 8.4%, from structure N to M. This result indicates that a suitable combination of nanoparticles and scattering particles is essential to improve the cell performance.

Both the transparent film composed of nanoparticles of 10–25 nm and the scattering film composed of large particles are not perfectly suitable for high light absorption; the former has no light-scattering effect and the latter has a smaller internal surface area and serious light loss due to back-scattering. Rothenberger et al. [23] established an optical model where a mixture of 65 wt.% transparent colloid and 35 wt.% scattering colloid could give the best gain in absorption. The gain of the mixture over transparent film was calculated to be 6% [23], which is in good agreement with the photocurrent increase of 5% from transparent to mixed film in this experiment. Since light scattering and the surface area depend on the particle size, the optimal mixture should be dependent on the large particle size. Ferber and Luther [21], concluded from computer simulations that the highest light absorption was obtained from an admixture of 5% large particles with radius 125–150 nm, which is different from our experimental result due to the different scattering particle size used.

The DSSC performance largely depends on the film thickness. Fig. 5 depicts the correlation between thickness and performance parameters obtained from structure M. J_{sc} increased from 11 to 18 μm but decreased with further increase in thickness r. Dye in the film will build up with increasing thickness, and an increased J_{sc} would be expected. The charge recombination between electrons injected from the excited dye to the conduction band of TiO_2 and the I_3^- ions in the electrolyte will, however, become more serious in thicker films, which is detrimental to electron collection on the back contact, and hence, photocurrent generation. One can see from the trend of J_{sc} that dye buildup dominates the photocurrent generation below 18 μm, resulting in an increase in J_{sc} until 18 μm. On the contrary, charge recombination plays a key role in the performance when the thickness is more than 18 μm. Contrary to the tendency of J_{sc}, V_{oc} decreased linearly with increasing film thickness. Charge recombination and mass transport limitations in the thicker film lead to a decreased V_{oc}. In addition, the series resistances of the thicker films grow quickly because the redox species and electrons migrate in a long path-length to complete the circuit. Balanced from J_{sc} and V_{oc}, η increased with thickness until 16 μm followed by a decrease. It is concluded from Fig. 5 that the optimal thickness falls in the range of 15–18 μm. The TiO_2 films present in this article had a thickness in the optimal range.

The charge recombination can be estimated by the magnitude and onset of dark current, which arises from the reduc-

Table 3
Performance of DSSCs with monolayer[a]

Type of structure	Adsorbed N719 ($\times 10^7$ mol cm^{-2})	J_{sc} (mA cm^{-2})	V_{oc} (mV)	FF	η (%)
N	2.15	14.86	727	0.705	7.62 ± 0.10
M	1.59	15.65	735	0.727	8.37 ± 0.15

[a] Open cells were measured under 100 mW cm^{-2} of simulated AM1.5 solar light.

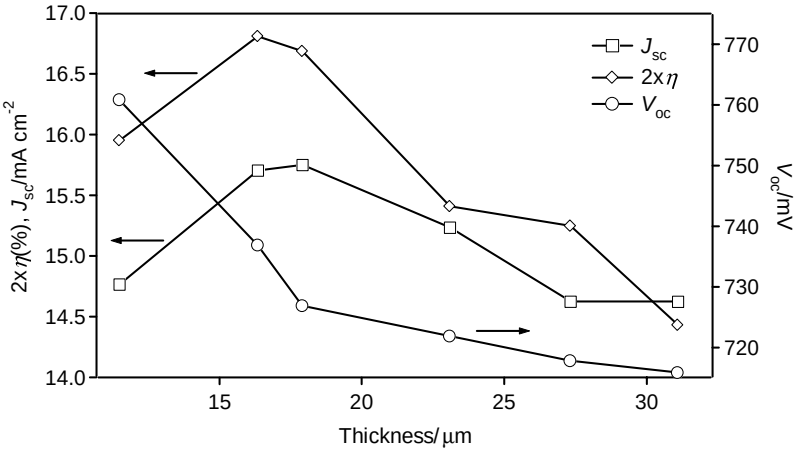

Fig. 5. Dependence of J_{sc}, V_{oc}, and η on the film thickness. The photoelectrodes in this figure had a structure of M. Open cells (not sealed) were tested under illumination of simulated AM1.5 solar light (100 mW cm^{-2}).

tion of I_3^- ions by the electrons on the conduction band. The dark current potential scan for photoelectrodes with structure M is plotted in Fig. 6. The dark current onset shifted to low potential with increasing thickness, and the thinner film produced a smaller dark current at the same potential above 0.6 V. These observations reflect a higher recombination rate between transported electrons and I_3^- ions in thicker films. The increase in the dark current with film thickness results in a loss in V_{oc}. Thus, V_{oc} decreases with increasing thickness.

Generally, high light absorption results directly from the thick films, but the series resistances of the cell and the dark currents should be minimized to get better performance. It is necessary to optimize the thickness while other factors limiting the cell performance are fixed. It is known that better absorption can be realized with thicker films from an optical point of view. However, it is very difficult to make porous film very thick without affecting its mechanical strength and the connectivity between particles. For a given photoelectrode, the optimal thickness depends on the extinction coefficient of adsorbed dye and as well as the particle properties.

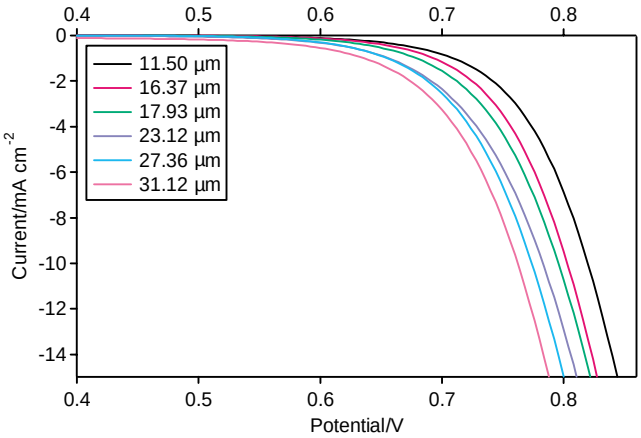

Fig. 6. Dark current vs. applied potential for open cells of M with various thicknesses.

While the optimal film thickness for N719 is in the range of 10–15 μm as reported in reference [21] or of 15–18 μm in this work, 5 μm TiO_2 film can generate a best efficiency for hemicyanine dyes [3,6]. The ideal case in DSSC is to employ a dye that has a very high extinction coefficient on a very thin porous film, which can produce both high photocurrent and high photovoltage, resulting in a higher efficiency.

3.2. Double layer

Compared to structure N, structure M showed a broader action spectrum and resulted in a better performance. However, the lower IPCEs in the range of 450–580 nm remind us that the IPCEs at the dye maximum absorption does not reach maximum for structure M (see Fig. 4). Increasing film thickness failed to improve the maximum IPCE and J_{sc} as discussed in the above section. The strong back-scattering of light due to the large particles near the conducting glass results unavoidably in a light loss, which may explain the fact that the maximum IPCE of M cannot reach unity as shown in Fig. 4. If the back-scattering of light is reduced or suppressed, maximum IPCE is expected to reach unity, and J_{sc} will, thus, be improved further.

In order to reduce or suppress the light loss ascribed to the back-scattering, double-layer-films (NS and NM) were tested. Since visible light can completely penetrate the transparent film, it is wise to deposit the nanoparticles first on the conducting glass followed by a second layer for light scattering. The back-scattering is expected to be suppressed in the double layer structure. Fig. 7 shows the action spectra of NS and NM. The spectrum of M is also shown in this figure for comparison. Compared with M, the significantly improved IPCEs below 620 nm in NS and NM are persuasive evidence for the efficient suppression of back-scattering. Contrary to the remarkable improvement of IPCEs below 620 nm, NS and NM gave lower IPCEs above 620 nm than M. For this reason, the J_{sc} was improved not so much from structure M to NS or NM as seen in Tables 3 and 4.

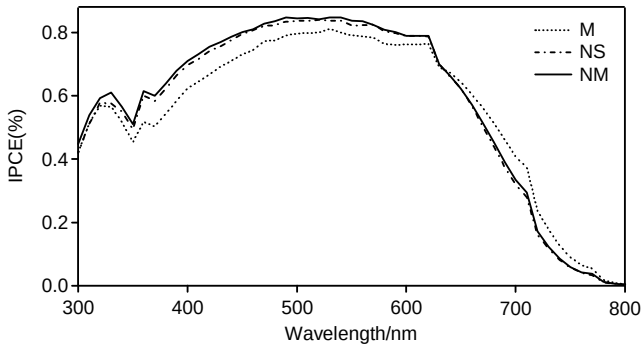

Fig. 7. Photocurrent action spectra of M, NS, and NM. Sealed cells were measured under 100 mW cm^{-2} illumination of AM1.5 simulated solar light; the same below.

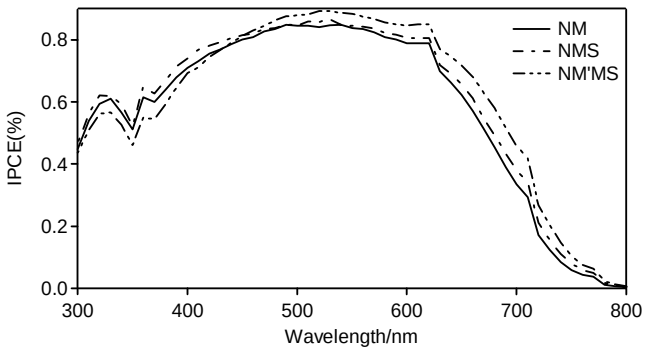

Fig. 8. Photocurrent action spectra of NM, NMS, and NM′MS.

For the two double layer structures, NM produces higher IPCEs than NS in the whole visible region. From structure NS to NM, the amount of large particles was decreased, which resulted in an increase of dye adsorption, as seen in Table 4. The similar IPCEs in the red region suggests that embedding of large particles in the matrix of nanoparticles will lead to a better light scattering than using large particles alone. NM, compared to NS, has a larger surface area while maintaining a similar light scattering, and therefore, produced a higher J_{sc}. The results for the performance of NS and NM are illustrated in Table 4. In agreement with the action spectra, NM gave a higher J_{sc} than NS. As a consequence, the overall yield of NM is also higher than that of NS. The overall yield is, therefore, increased from 8.4 to 9.2% by adjusting the film structure from monolayer M to double layer NM.

Besides the advantage of reducing absorption loss due to back-scattering, the configuration of NS is useful to enhance the light absorption in the front transparent layer by the backscattering from the top layer composed of large particles. The absorption gain of double layer over the first layer was calculated by Ferber and Luther [21] through computer simulations. Most recently, Grätzel's group employed such a configuration as NS for the study of DSSCs and obtained efficiencies in the range 8.4–8.6% [13,14], which are a little lower than the efficiency of NS in this work. They claimed that the second scattering layer is essential to get higher efficiencies, but they did not explain why these efficiencies are much lower than 10% reported in 1993 [7].

3.3. Multilayer

Although the double layer is better than the monolayer in terms of back-scattering suppression, the light-scattering effect in the double layer is not as efficient as in structure M; the IPCEs for the double layer are lower than those of M at the wavelength greater than 620 nm, as seen in Fig. 7. It is, therefore, imperative to increase the light scattering for the benefit of efficient red light harvesting. Since the path-depth length of light increases with wavelength, a better result should be obtained when the scattering centers are gradually increased. Therefore, a multilayer structure was proposed and tested. Fig. 8 shows the action spectra of NMS and NM′MS, where the spectrum of NM is also appended for comparison. NMS adsorbed a similar amount of dye to NM, but the former structure gave higher IPCEs in the visible range. The increased amount of light-scattering particles and the scattering center gradient may account for the enhanced IPCEs. As a result of improved IPCEs, J_{sc} was increased by 0.8 mA cm^{-2}, and η increased by 0.4%, as seen in Tables 4 and 5.

If too many large particles are incorporated into the film, the light absorption enhancement that results from light scattering can be offset by a lower dye concentration ascribed to a reduction of the total surface area. How to balance the surface area and the light scattering is the key to controlling the cell performance. Structure NM′MS could adsorb more dye than NMS, and present both higher IPCEs and broad feature. As a result, the DSSC with structure NM′MS yielded a higher efficiency, that is, 9.8% of η. The larger surface concentration of dye and the suitable light-scattering center

Table 4
Performance parameters of DSSC with double layer[a]

Type of structure	Adsorbed N719 ($\times 10^7$ mol cm^{-2})	J_{sc} (mA cm^{-2})	V_{oc} (mV)	FF	η (%)
NS	1.50	15.71	773	0.737	8.95 ± 0.10
NM	1.69	15.89	781	0.743	9.22 ± 0.05

[a] Sealed cells were measured under illumination of simulated AM1.5 solar light (100 mW cm^{-2}).

Table 5
Performance parameters for DSSCs with multilayers[a]

Type of structure	Adsorbed N719 ($\times 10^7$ mol cm^{-2})	J_{sc} (mA cm^{-2})	V_{oc} (mV)	FF	η (%)
NMS	1.54	16.74	776	0.742	9.64 ± 0.08
NM′MS	1.72	17.24	765	0.741	9.77 ± 0.12

[a] Sealed cells were measured under illumination of simulated AM1.5 solar light (100 mW cm^{-2}).

gradient in NM′MS may account for the higher IPCEs than those observed in NMS.

Fig. 9 shows the typical current–voltage characteristics of a sealed cell with structure NM′MS under illumination of simulated AM1.5 solar light (100 mW cm^{-2}). A thin anti-reflection layer was put on the cell surface to reduce the light reflection by the conducting glass. The J_{sc}, V_{oc}, and FF are 18.17 mA cm^{-2}, 764 mV, 0.737, respectively, corresponding to an overall energy conversion efficiency of 10.23%, which was reproduced many times. All the sealed DSSCs discussed here were very stable and sustained for at least 1 month with efficiency fluctuations of 0.2% within experimental error.

The overall efficiency of 10% for N719 was unmatched for several years until the discovery, in 2001, of the black dye which gave an efficiency of 10.4%. Most recently, Grätzel's group achieved a new record efficiency of 10.6 with N719 using guanidinium thiocyanate as additive in the electrolyte, which results in a remarkable improvement in the photovoltage [28]. We also broke the 10% record for N719 through tuning the layer structure while the other factors such as electrolyte and counter electrodes normally used in DSSCs were fixed. If the new electrolyte [28] and the new mode of Pt deposition [29] recently developed in Grätzel's group is applied in the multilayer configuration, it is expected to improve the efficiency further.

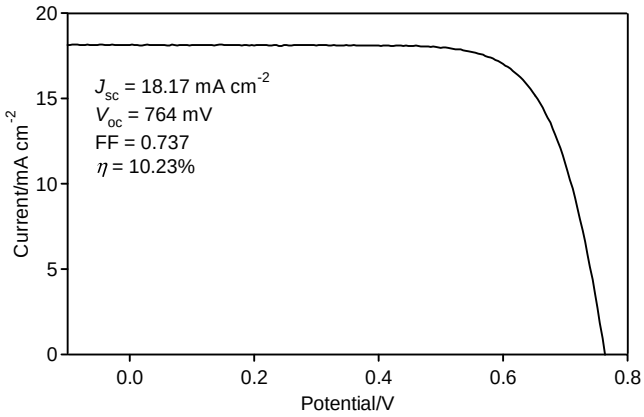

Fig. 9. Photocurrent–photovoltage characteristics of a sealed cell of NM′MS using an anti-reflection film layer on the cell surface to reduce the light reflection by the conducting glass.

4. Conclusions

It is evident that the cell performance depends on the film morphology for a given DSSC. Nanoparticles are essential to increase surface area, and hence, amount of dye, while large particles are required to enhance absorption of red light through light scattering. It is impossible to increase surface area and light scattering simultaneously, because they oppose each other. Therefore, there must be a balance between them. Such a balance was well controlled by tuning the layer structure, and an energy conversion efficiency of 10.2% was obtained using a multilayer structure. The multilayer structure is also suitable for other dyes in terms of improving light harvesting efficiency, and hence, photocurrent. In order to scatter the red light more efficiently, a more sophisticated multilayer structure with gradually increased particle size from the most-inner layer deserve to be constructed and tested. It is easy to control the film structure by screen printing. Consequently, such a simple but effective strategy may provide a way to improve the overall energy conversion efficiency even further.

Acknowledgements

This work was supported by the New Energy and Industrial Technology Development Organization (NEDO) under the Ministry of Economy Trade and Industry (METI).

References

[1] B. O'Regan, M. Grätzel, Nature (London) 353 (1991) 737.
[2] K. Hara, M. Kurashige, Y. Dan-Oh, C. Kasada, A. Shinpo, S. Suga, K. Sayama, H. Arakawa, New J. Chem. 27 (2003) 783.
[3] Z.-S. Wang, F.-Y. Li, C.-H. Huang, L. Wang, M. Wei, L.-P. Jin, N.-Q. Li, J. Phys. Chem. B 104 (2000) 9676.
[4] A. Islam, H. Sugihara, M. Yanagida, K. Hara, G. Fujihashi, Y. Tachibana, R. Katoh, S. Murata, H. Arakawa, New J. Chem. 26 (2002) 966.
[5] H. Zabri, I. Gillaizeau, C.A. Bignozzi, S. Caramori, M.-F. Charlot, J. Cano-Boquera, F. Odobel, Inorg. Chem. 42 (2003) 6655.
[6] Z.-S. Wang, F.-Y. Li, C.-H. Huang, J. Phys. Chem. B 105 (2001) 9210.
[7] M.K. Nazeeruddin, A. Kay, I. Rodicio, R. Humphry-Baker, E. Müller, P. Liska, N. Vlachopoulos, M. Grätzel, J. Am. Chem. Soc. 115 (1993) 6382.
[8] M.K. Nazeeruddin, P. Pechy, T. Renouard, S.M. Zakeeruddin, R. Humphry-Baker, P. Comte, P. Liska, C. Le, E. Costa, V. Shklover,

L. Spiccia, G.B. Deacon, C.A. Bignozzi, M. Grätzel, J. Am. Chem. Soc. 123 (2001) 1613.
[9] M. Yanagida, A. Islam, Y. Tachibana, G. Fujihashi, R. Katoh, H. Sugihara, H. Arakawa, New J. Chem. 26 (2002) 963.
[10] Z.-S. Wang, C.-H. Huang, B.-W. Zhang, Y.-J. Hou, P.-H. Xie, H.-J. Qian, K. Ibrahim, New J. Chem. 24 (2000) 567.
[11] T. Renouard, R.-A. Fallahpour, Md.K. Nazeeruddin, R. Humphry-Baker, S.I. Gorelsky, A.B.P. Lever, M. Grätzel, Inorg. Chem. 41 (2002) 367.
[12] H. Arakawa, Recent Advances in Research and Development for Dye-Sensitized Solar Cells, CMC, Tokyo, 2001, p. 28 (in Japanese).
[13] Md.K. Nazeeruddin, R. Splivallo, P. Liska, P. Comte, M. Grätzel, Chem. Commun. (2003) 1456.
[14] Md.K. Nazeeruddin, R. Humphry-Baker, P. Liska, M. Grätzel, J. Phys. Chem. B 107 (2003) 8981.
[15] Z.-S. Wang, C.-H. Huang, Y.-Y. Huang, Y.-J. Hou, P.-H. Xie, B.-W. Zhang, H.-M. Cheng, Chem. Mater. 13 (2001) 678.
[16] H. Kusama, H. Arakawa, J. Photochem. Photobiol. A: Chem. 160 (2003) 171.
[17] A. Hagfeldt, M. Grätzel, Chem. Rev. 95 (1995) 49.
[18] A. Zaban, S.G. Chen, S. Chappel, B.A. Gregg, Chem. Commun. (2000) 2231.
[19] E. Palomares, J.N. Clifford, S.A. Haque, T. Lutz, J.R. Durrant, J. Am. Chem. Soc. 125 (2003) 475.
[20] K. Tennakone, G.R.R.A. Kumara, I.R.M. Kottegoda, V.P.S. Perera, Chem. Commun. (1999) 15.
[21] J. Ferber, J. Luther, Sol. Energy Mater. Sol. Cells 54 (1998) 265.
[22] Y. Tachibana, K. Hara, K. Sayama, H. Arakawa, Chem. Mater. 14 (2002) 2527.
[23] G. Rothenberger, P. Comte, M. Grätzel, Sol. Energy Mater. Sol. Cells 58 (1999) 321.
[24] S.D. Burnside, V. Shklover, C. Barbé, P. Comte, F. Arendse, K. Brooks, M. Grätzel, Chem. Mater. 10 (1998) 2419.
[25] C.J. Barbé, F. Arendse, P. Comte, M. Jirousek, F. Lenzmann, V. Shklover, M. Grätzel, J. Am. Ceram. Soc. 80 (1997) 3157.
[26] N.-G. Park, J. van de Lagemaat, A.J. Frank, J. Phys. Chem. B 104 (2000) 8989.
[27] J. Desilvestro, M. Grätzel, L. Kaven, J. Moser, J. Am. Chem. Soc. 107 (1985) 2988.
[28] M. Grätzel, J. Photochem. Photobiol. C 4 (2003) 145.
[29] K. Kalyanasundaram, M. Grätzel, Coord. Chem. Rev. 77 (1998) 347.